



Research Article

Modal Proportion Analysis in Antenna Characteristic Mode Theory

Weiwen Li ¹, Yongcong Liu,¹ Jie Li,¹ Longfang Ye ² and Qing Huo Liu³

¹Department of Electronic Engineering, Xiamen University, Xiamen 361005, China

²Department of Electronic Science and Institute of Electromagnetics Acoustics, Xiamen University, Xiamen 361005, China

³Department of Electrical and Computer Engineering, Duke University, Durham, NC 27008, USA

Correspondence should be addressed to Weiwen Li; wvl@xmu.edu.cn

Received 6 November 2018; Accepted 11 December 2018; Published 13 February 2019

Academic Editor: Xiulong Bao

Copyright © 2019 Weiwen Li et al. This is an open access article distributed under the Creative Commons Attribution License, which permits unrestricted use, distribution, and reproduction in any medium, provided the original work is properly cited.

The characteristic mode theory (CMT) can provide physically intuitive guidance for the analysis and design of antenna structures. In CMT applications, the antenna current distribution is decomposed into the superposition of multiple characteristic modes, and the proportion of each current mode is characterized by the modal weighting coefficient (MWC). However, different characteristic currents themselves have different radiation efficiencies reflected by the eigenvalues. Therefore, from the perspective of the contribution to the radiation field, the modal proportion should be more accurately determined by the combination of the modal weighting coefficient and the mode current itself. Since the discrete mode currents calculated using the electromagnetic numerical method are distributed on the whole conductor surface, we can actually use the radiation field to quantify the modal proportion or estimate it using the far field in the maximum radiation direction. The numerical examples provided in the paper demonstrate that this modal proportion can effectively evaluate antenna performance.

1. Introduction

The characteristic mode theory (CMT) was first formulated by Garbacz in 1968 [1] and later refined by Harrington and Mautz in 1971 [2]. Characteristic modes are current modes that correspond to the eigenvectors of a particular weighted eigenvalue equation involving a generalized impedance matrix of the conductor. Hence, characteristic modes can be used to expand the total current on the conductor surface.

In fact, what makes characteristic modes really attractive for antenna design is the physical insight into antenna radiation. There is an eigenvalue or characteristic angle associated to each characteristic mode that can provide information about the mode resonance and radiating characteristics. Additionally, since characteristic modes only depend on the shape and size of the conducting object, antenna design can be performed in a controlled way.

However, CMT has once practically fallen into disuse. Later, in order to design and layout platform antennas [3, 4] and to obtain broadband and miniaturized mobile handset antennas [5], CMT has once again received attention. At

present, CMT has been widely used in terminal antennas, pattern reconfigurable antennas, and decoupling of multiple antennas [6–8].

When using CMT to design or analyze the antenna structure, we should first give the distributions of characteristic currents on the conductor surface. The selection of the feed point and the feed structure then has to be performed to excite the corresponding characteristic modes or combination thereof to meet the desired radiation field. For example, multiple CCEs (capacitive coupling elements) or ICEs (inductive coupling elements) are used to stimulate multiple modes of the mobile terminal to implement the MIMO antenna function [9, 10]. A circularly polarized radiation field is also achieved by exciting two orthogonal characteristic modes on the conductor plate [11, 12].

That is to say, to design an antenna is to stimulate the fundamental mode or the first few characteristic modes of the antenna structure and suppress the other modes as much as possible. Usually, the proportion level of each mode is characterized by the modal weighting coefficient (MWC) [10, 13]. Indeed, MWC can be used to select and determine

the feed point and feed structure for antenna design. However, since the radiation efficiency of each characteristic current is different [12], it is inaccurate to determine the proportion of this mode in the radiation field only by MWC. Therefore, the rationality of the antenna structure should be analyzed using the combination of MWC and mode current. We call this combination the modal proportion (MP).

Nevertheless, when the electromagnetic numerical calculation is used to determine the modal proportion, each characteristic current is discretely distributed on structure meshes, which makes it difficult to determine MP using mode currents. On the other hand, the far field of each mode is contributed by the overall current of the corresponding mode. Thus, it is proposed using the radiation field of the corresponding mode to quantify the modal proportion. We can also estimate the modal proportion using only field values in a certain spatial direction to verify that the design antenna is theoretically in compliance with the desired requirements.

2. Modal Weighting Coefficients

According to CMT, the actual current \mathbf{J} on the antenna conductor surface can be expressed as a linear superposition of characteristic mode currents \mathbf{J}_n :

$$\mathbf{J} = \sum_n \alpha_n \mathbf{J}_n, \quad (1)$$

where α_n is the MWC of the n th characteristic mode [2, 14].

On the ideal conductor surface, there is the relationship equation between the source and the field:

$$[Z(\mathbf{J}) - \mathbf{E}_{\text{tan}}^i] = 0, \quad (2)$$

where $Z(\cdot)$ describes the tangential component of the electric field due to the induced currents \mathbf{J} , and $\mathbf{E}_{\text{tan}}^i$ is the tangential component of the electric field incident on the conductor surface. Substitution of equation (1) into equation (2) yields

$$\sum_n \alpha_n Z(\mathbf{J}_n) - \mathbf{E}_{\text{tan}}^i = 0. \quad (3)$$

Then, the dot product of equation (3) and \mathbf{J}_m (m is any integer) produces

$$\sum_n \alpha_n \langle \mathbf{J}_m, Z\mathbf{J}_n \rangle - \langle \mathbf{J}_m, \mathbf{E}_{\text{tan}}^i \rangle = 0, \quad (4)$$

where the real and imaginary parts of the characteristic impedance $Z = R + jX$ are associated with the radiated and stored energy, respectively.

The characteristic modes can have the following orthogonality [2, 15]:

$$\langle \mathbf{J}_m^*, Z\mathbf{J}_n \rangle = (1 + j\lambda_n) \delta_{mn} = P(\mathbf{J}_m, \mathbf{J}_n), \quad (5)$$

where the symbol δ_{mn} is the Kronecker Delta, λ_n is the eigenvalue corresponding to mode n , and $P(\cdot)$ is the generated complex power.

Substituting equation (5) into equation (4), we can get

$$\alpha_n = \frac{\langle \mathbf{J}_n, \mathbf{E}_{\text{tan}}^i \rangle}{1 + j\lambda_n}. \quad (6)$$

It is seen that the modal weight coefficient α_n is a complex number.

In equation 6, $MS = |1/(1 + j\lambda_n)|$ is known as modal significance (MS), which is the intrinsic property of each mode and is independent of the external stimulus source [12, 16]. Quantitatively, the modal significance depends only on the eigenvalues. Since the radiation power is normalized to a unit value as shown in equation 5, there is $\lambda_n = \langle \mathbf{J}_n^*, X\mathbf{J}_n \rangle$, which presents the stored power. The smaller $|\lambda_n|$ is, the higher the radiation efficiency of the corresponding characteristic current \mathbf{J}_n . As λ_n is close to zero, the characteristic current \mathbf{J}_n exhibits resonant radiation. The modal significance converts the eigenvalue range of $[-\infty, +\infty]$ to its small range of $[0, 1]$.

The inner product $V_n^i = \langle \mathbf{J}_n, \mathbf{E}_{\text{tan}}^i \rangle$ of equation (6) is called the modal excitation coefficient (MEC) of mode n [2, 17]. Its value is proportional to the coupling degree between the n th mode and the externally incident field. This coupling level depends on the position, magnitude, phase, and polarization of the external excitation source. Thus, the modal excitation coefficient can be used to determine the feeding style and the feeding position.

If the feeding position is not appropriate, even the resonant eigenmode (λ_n close to zero) may not be excited. If the excitation point lies in a common location of two or more modes, the strong resonance mode (smaller $|\lambda_n|$) will be excited more strongly than the weak resonance mode (larger $|\lambda_n|$). In order to effectively stimulate mode n , the tangential component of the excitation electric field on the antenna surface should be consistent with the distribution direction of the characteristic current \mathbf{J}_n .

Along with the modal excitation coefficient, the modal significance measures the contribution of each mode to the overall electromagnetic response to some extent. It should be noted that the MWC shown in equation (6) has normalized the characteristic current of each mode by $\langle \mathbf{J}_n, R\mathbf{J}_n \rangle = 1$. Otherwise, the denominator of the modal weighting coefficient should be $\langle \mathbf{J}_n, R\mathbf{J}_n \rangle \cdot (1 + j\lambda_n)$ [18]. Thus, the amplitude of each characteristic current itself in equation (1) is different, though a different MWC has been applied for different mode currents.

In the numerical calculation of the electromagnetic field, the solved area must be discretized using the grids. At this time, the inner product of the vector in equation 6 is transformed into the inner product of the matrix. By applying the formula $\langle \alpha \cdot \beta \rangle = \beta^T \cdot \alpha$ for the inner product of matrices, where α or β denotes a column matrix and the superscript T denotes a complex conjugate transpose [19], we can obtain

the matrix form of the modal weighting coefficients:

$$\alpha_n = \frac{[V]^T [I]_n}{1 + j\lambda_n}, \quad (7)$$

where $[V]$ is an excitation source column matrix determined by the number of grids, and $[I]_n$ is a characteristic current column matrix of mode n determined by an eigenvalue equation. Therefore, the total current column matrix $[I]$ of the conductor surface can be expressed as

$$[I] = \sum_n \frac{[V]^T [I]_n}{1 + j\lambda_n} [I]_n. \quad (8)$$

3. Application of Modal Weighting Coefficient

After the current distribution of the first few characteristic modes with smaller eigenvalues is analyzed, the mode selection and combination are carried out with the desired antenna radiation field requirements. In that case, MWC is an important guiding parameter for the antenna design to determine the appropriate feed point and feed structure. Here, we illustrate the application of MWC with the radiation of a $50 \text{ mm} \times 30 \text{ mm}$ rectangular metal plate as an example.

3.1. Characteristic Modes. The eigenvalues of the first six modes for the rectangular metal plate within the frequency range from 1.0 GHz to 4.0 GHz are shown in Figure 1. It is seen that mode 1 can resonate effectively around 2.5 GHz. On the other hand, the eigenvalues of modes 3 and 6 are greater than zero, and thus they are induction modes that easily store magnetic energy.

The current distributions of the first six modes on the rectangular metal plate at 2.5 GHz are shown in Figure 2. We can see that mode 1 is a half-wave mode distributed along the long side, which is the fundamental mode, and mode 2 is a half-wave mode distributed along the short side. Mode 3 is an induction mode with a ring-shaped current. It can also be seen that mode 5 is the harmonic mode of mode 1, which means that these subsequent modes will be the higher order modes of the previous few modes. Therefore, it is sufficient to analyze only the first few modes.

The desired characteristic modes on a single conductor plate can be excited by magnetic field coupling or electric field coupling [10, 20]. A small conductor piece or probe placed above the rectangular conductor plate can excite electric fields parallel to the conductor plate. At this point, the corresponding modes of the conductor plate are generated by the electric field coupling and the excitation conductor piece is called the capacitive coupling element (CCE). Similarly, the ring-shaped structure on the conductor plate can be used to generate a ring-shaped current whose direction on the plate is the direction of the corresponding mode current. In that case, the magnetic field coupling is used to excite the corresponding characteristic mode and the excitation structure is called the inductive coupling element (ICE).

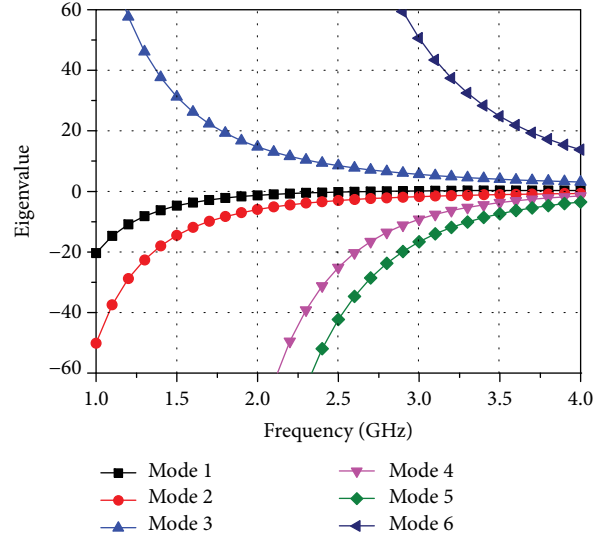


FIGURE 1: Eigenvalues of the first six modes for the $50 \text{ mm} \times 30 \text{ mm}$ rectangular metal plate.

The mode current distribution is consistent with that of the near-field magnetic field. Thus, the ICE should be placed at the maximum mode current or mode magnetic field position for good coupling. On the other hand, the CCE should be placed at the minimum point of the mode current or at the maximum position of the mode near-field electric field. To this end, Figure 3 shows the near-field electric field and near-field magnetic fields of the first two modes on the 5 mm plane above the metal plate.

3.2. Excitation Using CCE. According to the mode distributions shown in Figures 2 and 3, mode 1 can be excited using CCE and ICE, respectively. Figure 4(a) shows the schematic illustration of mode excitation by using a CCE piece, which is a $3 \text{ mm} \times 30 \text{ mm}$ rectangle placed 10 mm above the metal plate. Both ends of the voltage source connect the conductor plate and the metal piece, respectively.

The CCE size and position have a great influence on the coupling effect and port matching. The antenna return loss in this case is shown in Figure 4(b). We can observe that the antenna bandwidth is large, and its center frequency is at 2.25 GHz.

In order to determine whether mode 1 is effectively excited, the weighting coefficients of the first six modes are analyzed. Figure 4(c) shows the weighting values of the first 6 modes when the CCE is used. At this point, the voltage of the excitation source is taken as 1 V, and the subsequent analysis is also based on this setting. It should be noted here that the ordinal numbers of the modes are sorted by the eigenvalue magnitude. Whether the incentive structure exists or not can affect the serial number of some higher-order modes [21]. With reference to the characteristics of the current distribution and the feed structure, it can be seen that mode 4 in Figure 4(c) corresponds to mode 5 in Figure 2.

From Figure 4(c), it can be observed that mode 1 dominates in the operating frequency band. However, as the

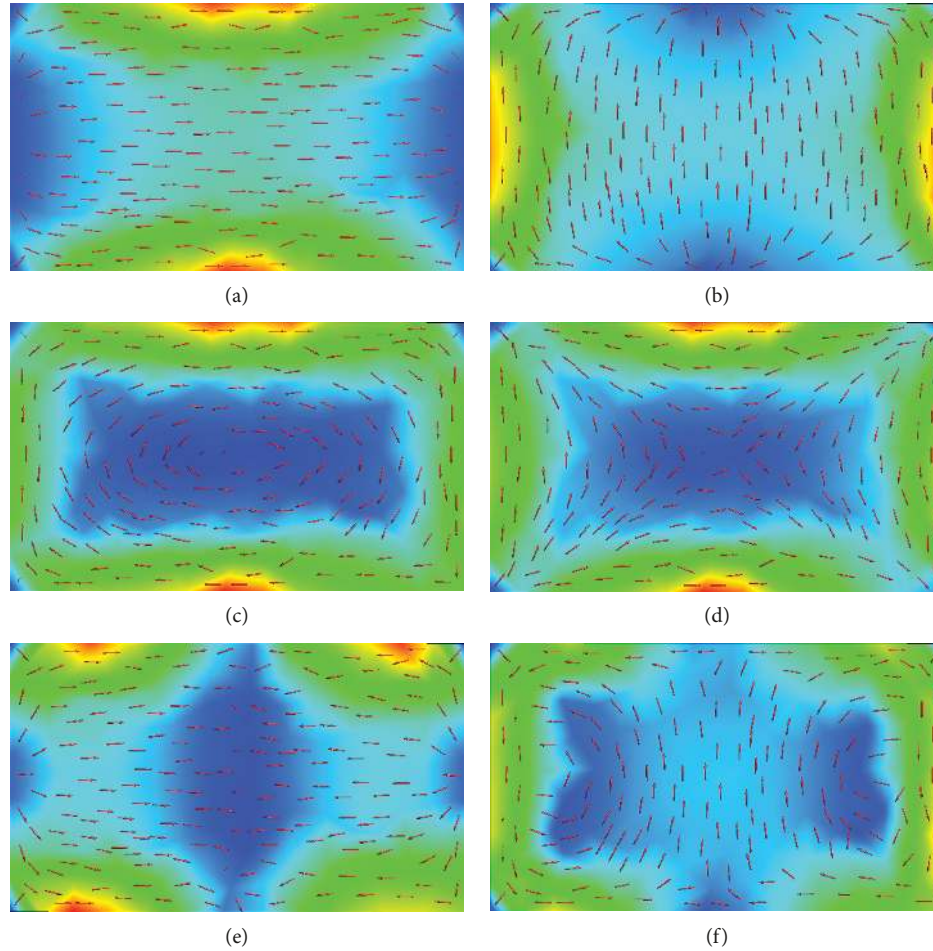


FIGURE 2: Characteristic currents for the first six modes of the rectangular metal plate at 2.5 GHz: (a) mode 1, (b) mode 2, (c) mode 3, (d) mode 4, (e) mode 5, and (f) mode 6.

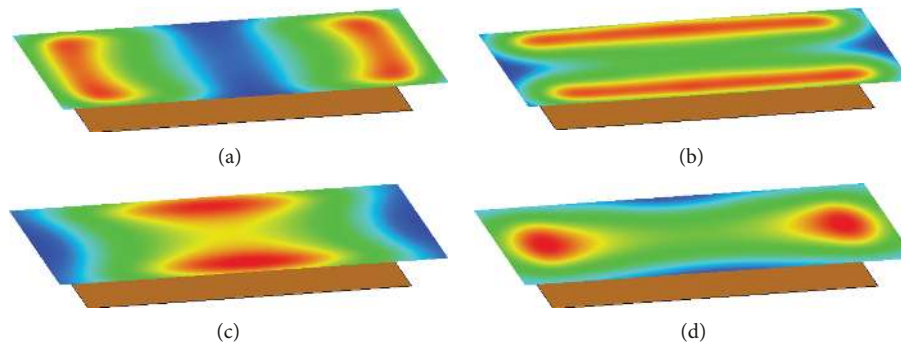


FIGURE 3: Normalized near-field map of the first two modes at 2.5 GHz for the rectangular metal plate: (a) electric field of mode 1, (b) electric field of mode 2, (c) magnetic field of mode 1, and (d) magnetic field of mode 2.

frequency increases, the proportion of mode 4 becomes large, even exceeding that of mode 1. This indicates that CCE excitation produces a low mode purity. Nevertheless, it is just the existence of dual-mode excitation that makes the antenna exhibit broadband characteristics.

3.3. Excitation Using ICE. As can be seen from Figure 3, the maximum magnetic field of mode 1 is in the middle of the

long side for the rectangular metal plate, and its main component should be the magnetic field in the z direction. Thus, the ICE constructed at the middle of the long side shown in Figure 5(a) can stimulate mode 1 by forming a nonresonant current loop. Here, the slit width is 0.5 mm, its length is 32 mm, and the spacing from the conductor edge is 0.5 mm. Due to the small size, the slit has little effect on the distribution of the original characteristic wave modes.

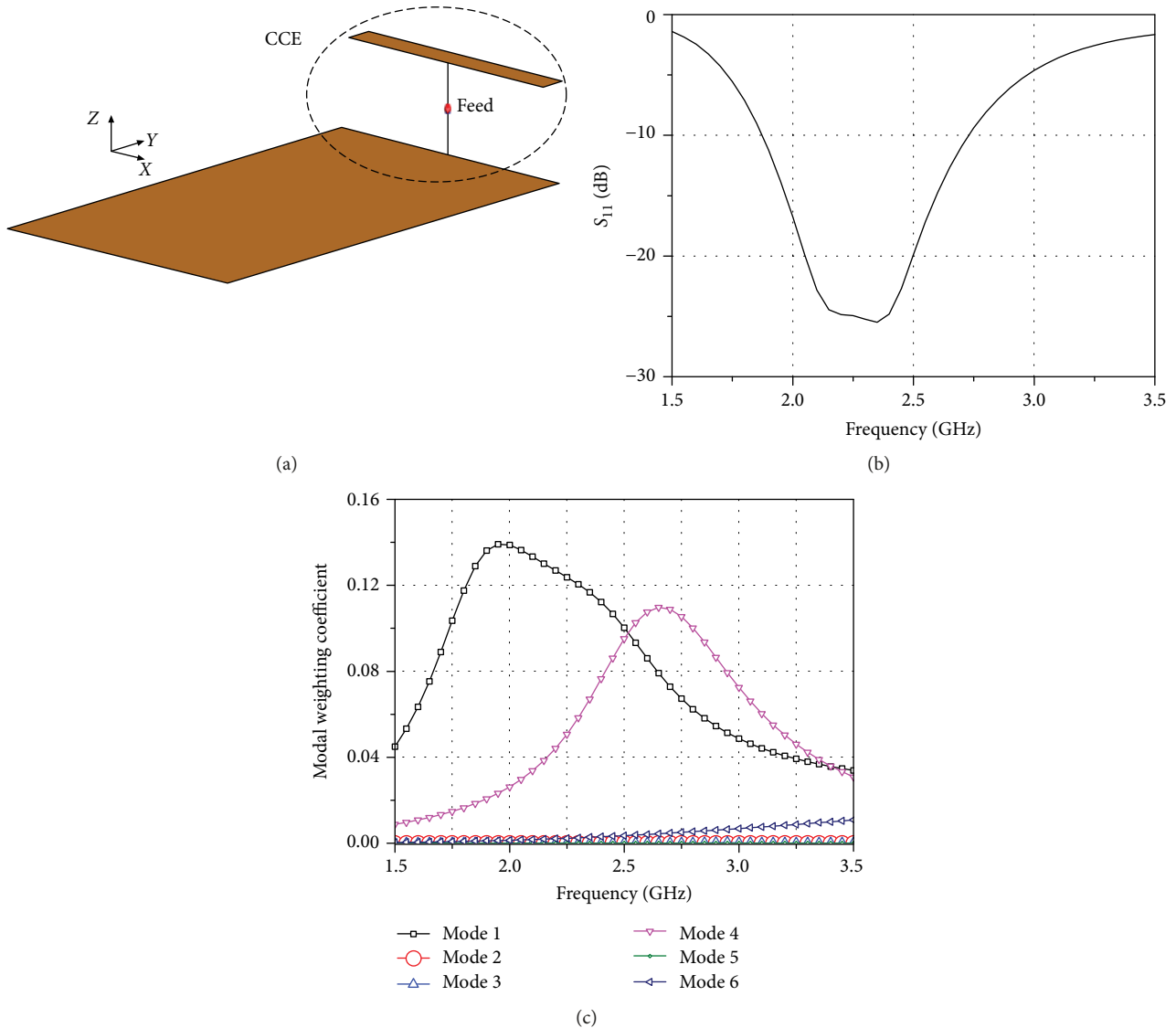


FIGURE 4: The rectangular metal plate excited using CCE and the corresponding S_{11} parameters and modal weighting coefficients: (a) schematic diagram of the CCE excitation, (b) S_{11} parameter, and (c) MWCs of the first six modes.

In order to match the excitation port, a capacitor of $C_f = 0.11$ pF is connected in a series, as shown in Figure 5(a). Figure 5(b) shows the return loss of the antenna using ICE excitation. It can be seen that the center frequency is at 2.2 GHz, and the bandwidth is greatly reduced relative to the case excited by using a CCE structure.

Figure 5(c) shows the modal weighting coefficients of the first six modes when ICE is used. We can see that mode 1 is effectively excited. Although the proportion of mode 3 is also large at this time, the purity of mode 1 is higher than that of the CCE excitation. It is consistent with the result pointed out in [22] that ICE usually excites a more purified single mode than CCE.

It should be noted that the solution of the eigenvalue equation is related to the frequency, so the amplitude of characteristic current at different frequencies is not the same. In fact, the oscillation of the mode current magnitude will

become more and more obvious with the increase of frequency, which is also reflected in Figure 5(c). However, the relative relationship of characteristic currents between modes does not change with frequency. Therefore, for the normalized characteristic modes, the influence of the current amplitude change can be basically ignored.

4. Modal Proportion

4.1. Mode Contribution Based on Characteristic Currents. The MWC analysis has utilized the orthogonality of the characteristic current wave mode, and each mode radiation power is first normalized to the unit value. On the other hand, the reactive power is proportional to the eigenvalue magnitude. Thus, the amplitude of a characteristic current is related to the radiation efficiency of the corresponding mode, i.e., its eigenvalue magnitude. Higher-order modes

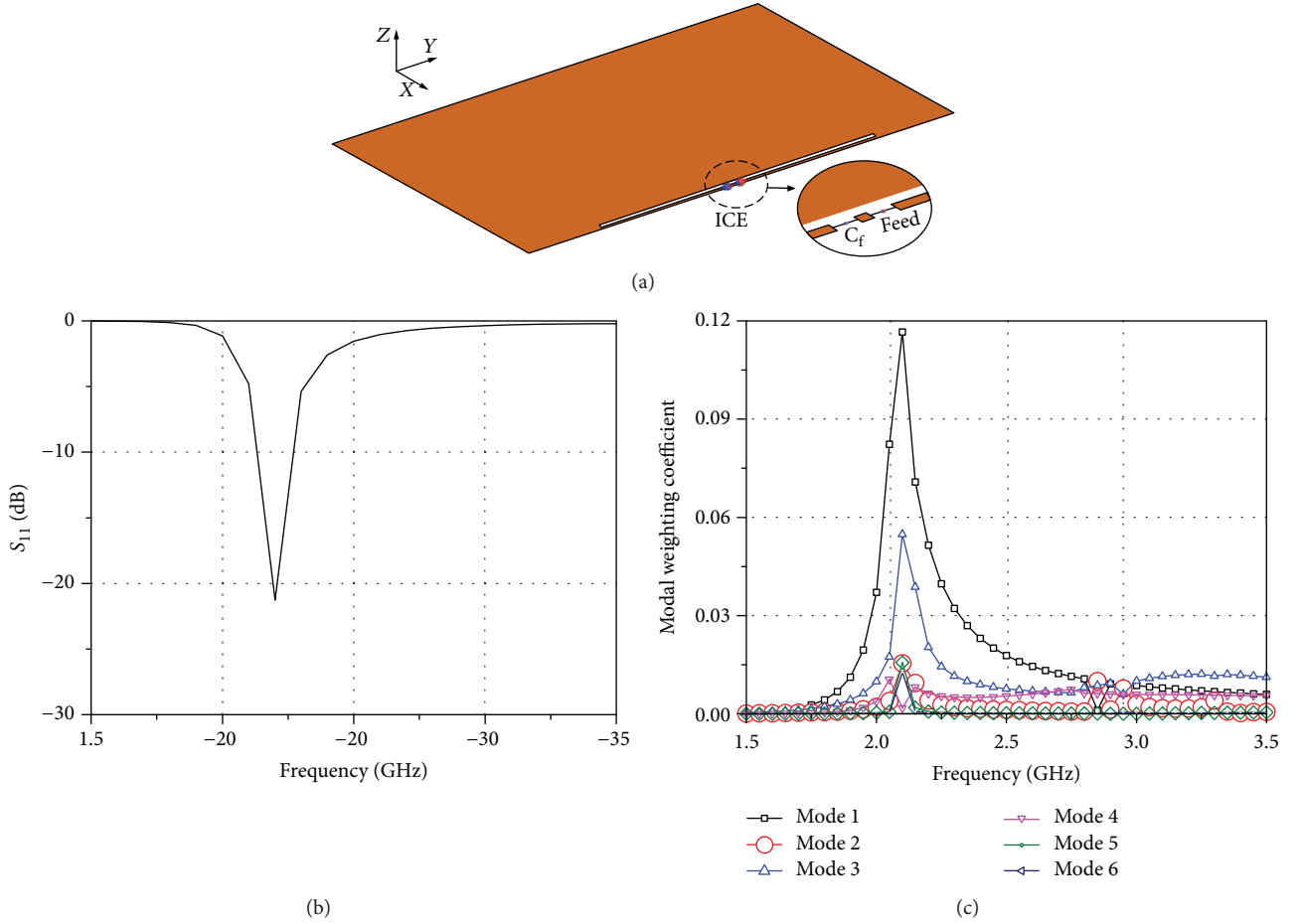


FIGURE 5: The rectangular metal plate excited using ICE and the corresponding S_{11} parameter and modal weighting coefficients: (a) schematic diagram of ICE excitation, (b) S_{11} parameter, and (c) MWCs of the first six modes.

require large mode currents to reach the same unit radiation power level as lower-order modes.

That is, the amplitudes of the expanding respective characteristic currents on the open conductor are not equal. On this basis, the modes are weighted in equation (1). Therefore, only using MWC α_n to indicate each mode contribution to the total radiation field is not complete. The MWC curves of Figures 4(c) and 5(c) do not fully reflect the excited degree of mode 1. It should be the result of multiplying the weighting coefficient and the mode current, to truly reflect the modal proportion.

If the modal weighting coefficient is calculated using the mode current normalized by input power rather than radiation power, the actual proportion of the corresponding mode can be correctly determined by MWC squared [13]. In fact, this kind of mode proportion is considered from the power point of view, and the corresponding calculation amount increases. Therefore, we consider the modal proportion by combining MWC and the mode current itself.

According to equation (1), by the numerical method the total current at the antenna surface can be expressed as

$$[I] = \alpha_1[I]_1 + \alpha_2[I]_2 + \alpha_3[I]_3 + \dots + \alpha_n[I]_n, \quad (9)$$

where $[I]$ is an $N \times 1$ current matrix on N grids, and n is the mode number. $\alpha_n[I]_n$ is then the contribution of mode n to the total surface current.

In general, only a few lower order modes play a major role in the radiation field. The number of modes can be selected according to the modal significance being greater than $1/\sqrt{2}$ or the eigenvalue value being less than 1. For the conductor plate involved in Section 3, the higher-order modes have basically been suppressed owing to the coupling characteristics of the feed structures. Therefore, only the first six modes are used for the approximate calculation of mode radiation. However, since the current distributions have the vector characteristics, it is troublesome to calculate the mode proportion using discrete modal currents.

4.2. Mode Contribution Based on Far Fields. Each characteristic mode current of the antenna structure produces a corresponding radiation pattern of the far field. The proportion of the far field to the total radiation field in this mode is the same as the proportion of the mode current in the total current. Therefore, the corresponding modal proportion of the antenna can be verified by the proportion of the radiated field. The total electric field \mathbf{E} of the far field can be

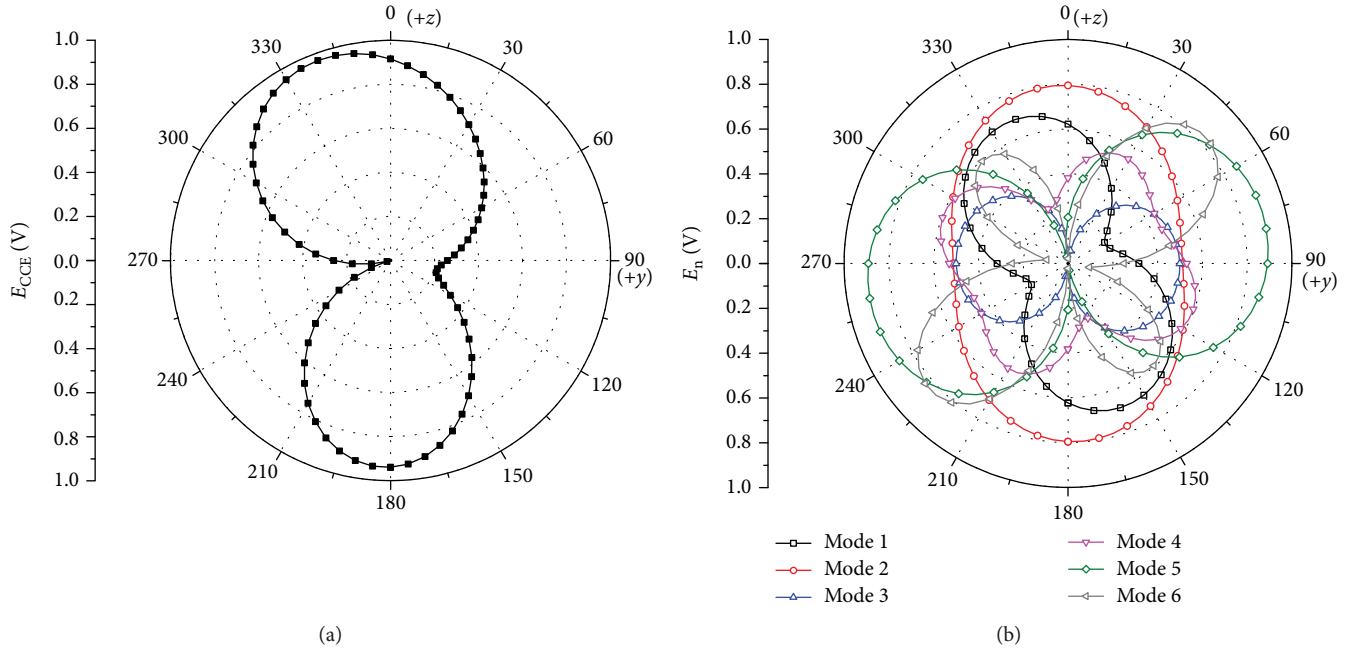


FIGURE 6: Radiation patterns of the total field and the first six modes for the CCE-fed antenna on the yoz plane of $\varphi = 90^\circ$ at 2.2 GHz: (a) total field using the full-wave method and (b) far field for the first six modes.

represented by a linear superposition of the electric field \mathbf{E}_n of each mode as [2]

$$\mathbf{E} = \sum_n \alpha_n \mathbf{E}_n. \quad (10)$$

Similarly, the actual radiation field is mainly determined by the first few modes, and only the first 6 modes are also analyzed for the antennas shown in Figures 4(a) and 5(a).

However, it should be noted that the radiation field of each mode has directionality. The calculation of the modal proportion should use the integrated value of the corresponding mode energy flow density on the enclosing surface surrounding the antenna. If so, the calculation process is also complicated. However, since the antenna total radiation field is mainly determined by the first one or two modes [15], the directivity of the total field is similar to that of these modes. Thus, the maximum radiation direction of the total field is selected, and the field values of each mode are extracted from the selected direction. Combined with MWC, the analysis of the modal proportion can then be performed.

For a specific calculation, the maximum radiation direction of the main mode or total far-field electric field is firstly obtained by the full-wave method. Then, a cut plane containing the maximum field is selected, the radiation pattern of each mode on this plane is given, and the field value of each mode in the maximum radiation direction is read. Combined with the modal weighting coefficient, the proportion of the corresponding mode is estimated using equation (10). Here, it is important to choose the spatial direction in which field values can be extracted for calculation.

4.3. Mode Proportion for CCE-Fed Antenna. For the antenna in Figure 4(a) based on the CCE feed, the radiation pattern of

the total far-field electric field on the $\varphi = 90^\circ$ plane at 2.2 GHz is shown in Figure 6(a), and the patterns of the first 6 modes on this plane are shown in Figure 6(b). It can be seen that mode 4 in Figure 6(b) corresponds to mode 5 of Figure 2, which further confirms the analysis result of mode 4 in Figure 4(c).

In Figure 6(a), the maximum field direction is at $\theta = 340^\circ$. In this direction, the total field value in Figure 6(a) and the field values of each mode in Figure 6(b) are all extracted and listed in Table 1. MWCs for each mode shown in Figure 4(c) are also provided in Table 1. According to equation (10), the total electric field value in the maximum radiation direction then is

$$E_{\text{CCE}} \approx \alpha_1 E_1 + \alpha_2 E_2 + \dots + \alpha_6 E_6 = 0.985 \text{ mV}. \quad (11)$$

At this point, the proportion of mode 1 is $\alpha_1 E_1 / E_{\text{CCE}} \approx 83.5\%$, and the proportion of mode 4 is about 15.2%. However, the mode contribution determined only by MWC is 66.4% for mode 1 and 32.0% for mode 4.

Under the condition that the excitation source voltage is 1 V, the total electric field value (0.985 mV) calculated by the first six modes in the maximum radiation direction is substantially the same as the value (0.967 mV) of Figure 6(a) directly determined by the full-wave method. This result implies that the modal proportion analysis using the far field in the maximum direction is feasible. On the other hand, this further confirms that the total radiation power of the antenna is basically contributed by the first few modes.

4.4. Mode Proportion for ICE-Fed Antenna. For the antenna based on the ICE feed in Figure 5(a), the distribution of the total far-field electric field on the $\varphi = 0^\circ$ plane at 2.2 GHz is

TABLE 1: MWCs and far field values ($\theta = 340^\circ$ and $\varphi = 90^\circ$) of the first 6 modes of CCE-fed antenna at 2.2 GHz.

| Mode | MWC from Figure 4(c) | MWC proportion | EFV from Figure 6(b) | MWC \times EFV | Modal proportion |
|------|----------------------|----------------|----------------------|------------------|------------------|
| 1 | 0.120 | 66.3% | 6.849 | 0.822 | 83.5% |
| 2 | 0 | 0 | 7.715 | 0 | 0 |
| 3 | 0 | 0 | 2.518 | 0 | 0 |
| 4 | 0.058 | 32% | 2.589 | 0.150 | 15.2% |
| 5 | 0 | 0 | 1.814 | 0 | 0 |
| 6 | 0.003 | 1.7% | 4.448 | 0.013 | 1.3% |

MWC, modal weighting coefficient; EFV, electric field value.

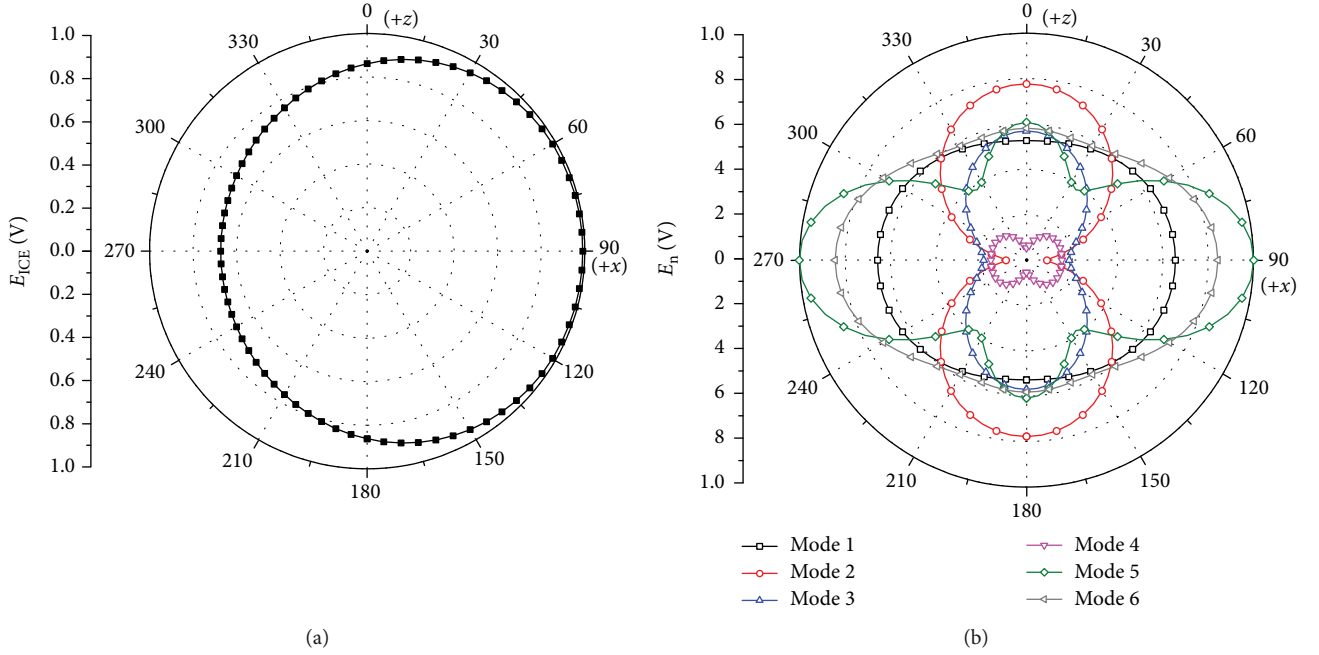


FIGURE 7: Radiation patterns of the total field and the first six modes for the ICE-fed antenna on the xoz plane of $\varphi = 0^\circ$ at 2.2 GHz: (a) total field using the full-wave method and (b) far field for the first six modes.

shown in Figure 7(a). The radiation patterns of the first 6 modes on the same plane are shown in Figure 7(b).

The field values for each mode in the maximum radiation direction ($\theta = 90^\circ$, $\varphi = 0^\circ$) are extracted from Figure 7, and the weighting coefficients of the respective modes are read from Figure 5(c). All these data are listed in Table 2. Then, it can be obtained that the total electric field value in the maximum radiation direction is

$$E_{\text{ICE}} \approx \alpha_1 E_1 + \alpha_2 E_2 + \dots + \alpha_6 E_6 = 1.158 \text{ mV}. \quad (12)$$

At this time, mode 1 accounts for about $\alpha_1 E_1 / E_{\text{ICE}} \approx 66.3\%$, while modes 3, 5, and 6 also have a large proportion. However, the proportion (66.3%) of mode 1 is greater than the value (53.7%) determined by MWC, indicating that antenna radiation is still mainly contributed by mode 1. The total electric field value in the maximum radiation direction calculated by the first six modes is 1.158 mV, while that obtained by full wave analysis is 1.001 mV, which is also close to the former.

We can also observe that the proportion of mode 1 in the CCE-fed antenna is larger than that in the ICE-fed antenna.

This coincides with the conclusion that the radiation efficiency of the capacitive coupling antenna is greater than that of the inductive coupling antenna. It indicates that the modal proportion can also reflect the antenna radiation efficiency to some extent.

In summary, in order to determine the contribution of a certain mode to total radiation, using the modal proportion calculated by the far-field electric field is more reasonable than using MWC. However, there are two main error sources for the modal proportion calculation using far fields. One is that the antenna radiation fields are approximated by the electric field in the maximum direction, and the other is introduced by the numerical calculation. The final error can be estimated by the difference between the total field calculated by each mode and that directly obtained by the full-wave method. Thus, the relative error for the above CCE-fed antenna is about 1.9% and that for the ICE-fed structure is approximately 15.7%, which is relatively large. The reason is that the antenna structure using the ICE excitation has a poor ability to suppress high-order modes. From this point of view, it cannot be said that it is easier to use ICE than CCE to achieve a high purity mode.

TABLE 2: MWCs and far field values ($\theta = 90^\circ$ and $\varphi = 0^\circ$) of the first 6 modes of the ICE-fed antenna at 2.2 GHz.

| Mode | MWC from Figure 5(c) | MWC proportion | EFV from Figure 7(b) | MWC \times EFV | Modal proportion |
|------|----------------------|----------------|----------------------|------------------|------------------|
| 1 | 0.117 | 53.7% | 6.564 | 0.768 | 66.3% |
| 2 | 0.015 | 6.9% | 0.903 | 0.014 | 1.2% |
| 3 | 0.055 | 25.5% | 1.881 | 0.103 | 8.9% |
| 4 | 0.002 | 0.9% | 1.563 | 0.003 | 0.3% |
| 5 | 0.016 | 7.3% | 10.014 | 0.160 | 13.8% |
| 6 | 0.013 | 6.0% | 8.431 | 0.011 | 9.5% |

MWC, modal weighting coefficient; EFV, electric field value.

5. Conclusion

The application of the characteristic mode theory in antenna structures is to decompose and synthesize surface currents or radiation fields. As the radiation field is decomposed into the superposition of orthogonal modes, the antenna performance is easy to optimize and realize from the physical principle. Each characteristic mode contribution to the total antenna performance cannot be determined only by the modal weighting coefficient, because different characteristic currents have different radiation efficiencies reflected by the eigenvalues. The modal proportion should be calculated by the combination of the modal weighting coefficient and mode current. However, the extraction of discrete mode currents is cumbersome in electromagnetic numerical methods. Therefore, we use the far field in the maximum radiation direction to quantify the modal proportion. This modal proportion can effectively evaluate the antenna performance.

Data Availability

The data used to support the findings of this study are included within the article.

Conflicts of Interest

The authors declare that they have no conflicts of interest.

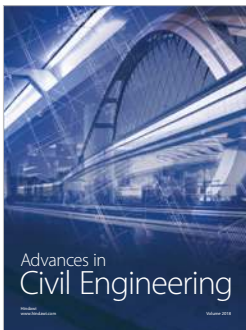
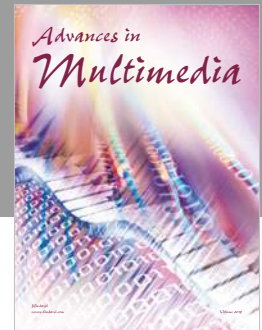
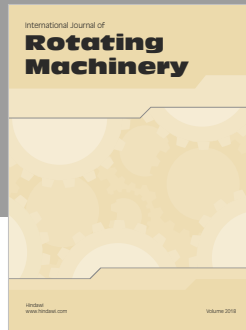
Funding

This work was supported by the Open Fund of the State Key Laboratory on Integrated Optoelectronics (IOSKL2017 KF02), China.

References

- [1] R. J. Garbacz, "Modal expansions for resonance scattering phenomena," *Proceedings of the IEEE*, vol. 53, no. 8, pp. 856–864, 1965.
- [2] R. Harrington and J. Mautz, "Theory of characteristic modes for conducting bodies," *IEEE Transactions on Antennas and Propagation*, vol. 19, no. 5, pp. 622–628, 1971.
- [3] K. P. Murray and B. A. Austin, "Synthesis of vehicular antenna NVIS radiation patterns using the method of characteristic modes," *IEE Proceedings - Microwaves, Antennas and Propagation*, vol. 141, no. 3, pp. 151–154, 1994.
- [4] B. A. Austin and K. P. Murray, "The application of characteristic-mode techniques to vehicle-mounted NVIS antennas," *IEEE Antennas and Propagation Magazine*, vol. 40, no. 1, pp. 7–21, 30, 1998.
- [5] E. Antonino-Daviu, C. A. Suarez-Fajardo, M. Cabedo-Fabres, and M. Ferrando-Bataller, "Wideband antenna for mobile terminals based on the handset PCB resonance," *Microwave and Optical Technology Letters*, vol. 48, no. 7, pp. 1408–1411, 2006.
- [6] H. Li, Z. T. Miers, and B. K. Lau, "Design of orthogonal MIMO handset antennas based on characteristic mode manipulation at frequency bands below 1 GHz," *IEEE Transactions on Antennas and Propagation*, vol. 62, no. 5, pp. 2756–2766, 2014.
- [7] K. K. Kishor and S. V. Hum, "A pattern reconfigurable chassis-mode MIMO antenna," *IEEE Transactions on Antennas and Propagation*, vol. 62, no. 6, pp. 3290–3298, 2014.
- [8] H. Li, B. K. Lau, Z. Ying, and S. He, "Decoupling of multiple antennas in terminals with chassis excitation using polarization diversity, angle diversity and current control," *IEEE Transactions on Antennas and Propagation*, vol. 60, no. 12, pp. 5947–5957, 2012.
- [9] K. K. Kishor and S. V. Hum, "Multiport multiband chassis-mode antenna design using characteristic modes," *IEEE Antennas and Wireless Propagation Letters*, vol. 16, pp. 609–612, 2017.
- [10] R. Martens and D. Manteuffel, "Systematic design method of a mobile multiple antenna system using the theory of characteristic modes," *IET Microwaves, Antennas & Propagation*, vol. 8, no. 12, pp. 887–893, 2014.
- [11] Y. Chen and C.-F. Wang, "Characteristic-mode-based improvement of circularly polarized U-slot and E-shaped patch antennas," *IEEE Antennas and Wireless Propagation Letters*, vol. 11, pp. 1474–1477, 2012.
- [12] M. Cabedo-Fabres, E. Antonino-Daviu, A. Valero-Nogueira, and M. Bataller, "The theory of characteristic modes revisited: a contribution to the design of antennas for modern applications," *IEEE Antennas and Propagation Magazine*, vol. 49, no. 5, pp. 52–68, 2007.
- [13] E. Safin and D. Manteuffel, "Reconstruction of the characteristic modes on an antenna based on the radiated far field," *IEEE Transactions on Antennas and Propagation*, vol. 61, no. 6, pp. 2964–2971, 2013.
- [14] P. Hazdra and P. Hamouz, "On the modal superposition lying under the MoM matrix equations," *Radioengineering*, vol. 17, no. 3, pp. 42–46, 2008.
- [15] R. Harrington and J. Mautz, "Computation of characteristic modes for conducting bodies," *IEEE Transactions on Antennas and Propagation*, vol. 19, no. 5, pp. 629–639, 1971.
- [16] J. L. T. Ethier and D. A. McNamara, "Modal significance measure in characteristic mode analysis of radiating structures," *Electronics Letters*, vol. 46, no. 2, pp. 107–108, 2010.

- [17] E. Antonino-Daviu, M. Fabres, M. Ferrando-Bataller, and V. M. R. Penarrocha, "Modal analysis and design of band-notched UWB planar monopole antennas," *IEEE Transactions on Antennas and Propagation*, vol. 58, no. 5, pp. 1457–1467, 2010.
- [18] C. T. Famide, W. L. Schroeder, and K. Solbach, "Numerical analysis of characteristic modes on the chassis of mobile phones," in *2006 First European Conference on Antennas and Propagation*, pp. 358–361, Nice, France, November 2006.
- [19] D. Liu, R. J. Garbacz, and D. M. Pozar, "Antenna synthesis and optimization using generalized characteristic modes," *IEEE Transactions on Antennas and Propagation*, vol. 38, no. 6, pp. 862–868, 1990.
- [20] R. Martens, E. Safin, and D. Manteuffel, "Selective excitation of characteristic modes on small terminals," in *Proceedings of the 5th European Conference on Antennas and Propagation (EUCAP)*, pp. 2492–2496, Rome, Italy, April 2011.
- [21] K. K. Kishor and S. V. Hum, "A two-port chassis-mode MIMO antenna," *IEEE Antennas and Wireless Propagation Letters*, vol. 12, pp. 690–693, 2013.
- [22] Z. Liang, J. Ouyang, F. Yang, and L. Zhou, "Design of license plate RFID tag antenna using characteristic mode pattern synthesis," *IEEE Transactions on Antennas and Propagation*, vol. 65, no. 10, pp. 4964–4970, 2017.



Hindawi

Submit your manuscripts at
www.hindawi.com

